# Novel Compact Filtering Power Divider with Harmonic Suppression

**Wei-Qiang Pan[1], Jin-Xu Xu[2, *], Qian Fei Su[3], and Xiao-Lan Zhao[2]**

**Abstract**—This paper presents a novel power divider with filtering responses. By using quarter-wavelength resonators with a novel feeding structure, both power division and bandpass responses are obtained, and compact size is realized. Discriminating coupling is utilized to suppress the third harmonic to obtain wide stopband. The isolation resistor is connected at two ends of the input feed line, and good isolation is obtained. Two transmission zeros are generated at two edges of the passband, resulting in high selectivity. For demonstration, a filtering power divider is implemented. Comparisons of the measured and simulated results are presented to verify the theoretical predications.

## 1. INTRODUCTION

In RF front-ends, power dividers and bandpass filters (BPFs) are vital blocks. They can be used to split the input energy and reject the unwanted signals. Therefore, they have attracted much research interest, and various methods have been proposed to design various applications. In [1–4], multi-band power dividers, ultra-wideband power divider and unequal power divider are realized with different methods. In [5–7], multi-band bandpass filters, wideband filter and tunable filter are designed by multi-mode and multi-set of resonators. However, in conventional designs, they are usually individually designed and connected by a $50\,\Omega$ transmission line, which occupies large area and has high insertions. Therefore, it is necessary to integrate the two functions into one device [8–16].

In [8], $\Pi$ shape transmission lines are designed with $90°$ phase shift and specific characteristic impedance to replace quarter-wavelength lines in Wilkinson power divider. However, it suffers poor selectivity. To improve the selectivity, open loop resonators are utilized. These resonators exhibit $90°$ phase shift at the center frequency, ensuring their exchange with quarter-wavelength lines. Using this method, single and dual-band power dividers with filtering function are designed [9]. In [10, 11], power divider integrated bandpass responses are realized with high selectivity. Unfortunately, they occupy large areas since they utilized half-wavelength resonators. To reduce the size, quarter-wavelength resonators are used. In [12], a symmetric third-order coupling structure is used to create power division and filtering functions as well as enhanced suppression at the second harmonic. In [13], folded quarter-wavelength stepped-impedance resonators are employed. By controlling the impedances, the harmonic can be removed far away from the passband. Unfortunately, they suffer from large insertion loss and poor selectivity. Besides equal narrow bandwidth filtering power dividers, the unequal and wideband power dividers with filtering responses are also investigated [14–16].

In this paper, a novel filtering power divider with harmonic suppression is proposed. It employs quarter-wavelength resonators, resulting in compact size. The resistor is connected at the ends of the input feed line, resulting in good isolation. By controlling the coupling region, the third harmonic can be effectively suppressed. Meanwhile, transmission zeros are generated at both sides of the passband, ensuring high selectivity. For demonstration, a compact power divider is implemented, with the theoretical analysis and experimental results presented.

## 2. STUB-LOADED QUARTER-WAVELENGTH RESONATOR

Figure 1 shows the proposed microstrip filtering power divider with harmonic suppression. It consists of two identical coupled-line sections and a resistor. Each part is composed of a quarter-wavelength resonator and input/output feed lines. The circuit is symmetrical, allowing even- and odd-mode analysis. Based on the odd-even mode theory, the S-matrix of the circuit can be expressed as follows [17]

$$[S] = \begin{bmatrix} S_{11e} & \dfrac{1}{\sqrt{2}}S_{21e} & \dfrac{1}{\sqrt{2}}S_{21e} \\[2mm] \dfrac{1}{\sqrt{2}}S_{21e} & \dfrac{1}{2}\left(S_{22e}+S_{22o}\right) & \dfrac{1}{2}\left(S_{22e}-S_{22o}\right) \\[2mm] \dfrac{1}{\sqrt{2}}S_{21e} & \dfrac{1}{2}\left(S_{22e}-S_{22o}\right) & \dfrac{1}{2}\left(S_{22e}+S_{22o}\right) \end{bmatrix} \tag{1}$$

where the symbol $e$ and $o$ correspond to the even- and odd-mode equivalent sub-circuits, respectively. To realize filtering power division responses, $S_{21e}$ should be equivalent to the transmission coefficient of a BPF. Meanwhile, $S_{11e}$, $S_{22e}$ and $S_{22o}$ should be zero to obtain good port matching and high isolation.

For the even-mode circuit, it is a three-line coupled structure as shown in Figure 2(a), which can be treated as a BPF with two different feed lines. The middle short-ended microstrip line acts as a quarter-wavelength resonator and the length $L_4$ determines the operating frequency [18]. For the bandwidth, it is mainly controlled by the coupling strength among the three coupled lines. Small coupling gaps result in wide bandwidth. Figure 3 shows the simulated $|S_{21e}|$ against $G_4$. It can be observed that when $G_4$ decreases, the bandwidth becomes wide.
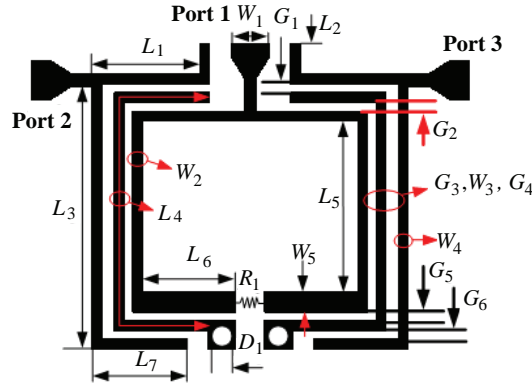


**Figure 1.** Configuration of the proposed filtering power divider.
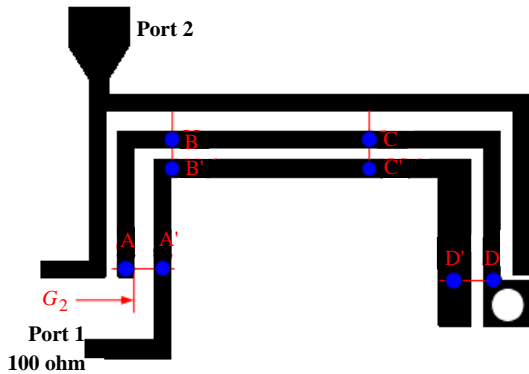


**Figure 2.** Even-mode circuit.
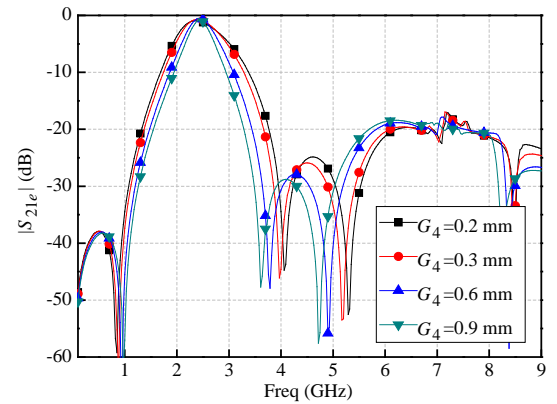
**Figure 3.** Simulated $|S_{21e}|$ against $G_4$.

To suppress the harmonic, discriminating coupling is utilized [19], and the coupling region between the feeding line and resonator should be properly selected. The coupling strength can be investigated by studying the voltage and current distribution within the coupling region [19]. As illustrated in Figure 2, the resonator can be equally divided into three parts, A to B, B to C and C to D. For the feed line, the end is open and the reflection coefficient is 1, thus standing wave can be formed on the feed line. For the resonator, standing wave is also realized at the fundamental and third harmonic frequency. Thus, the current within the coupling region can be simply illustrated in Figure 4(a). $I_{R,f}$ and $I_{R,3f}$ denote the current distribution of fundamental and third harmonic of the resonator. $I_{F,f}$ and $I_{F,3f}$ denote the current distribution of fundamental and third harmonic of the input feed line. The overall coupling coefficient is the sum of electric and magnetic coupling coefficients $k_e$ and $k_m$

$$k = k_e + k_m \tag{2}$$

$k_m$ can be defined as follows [19]:

$$k_m = \frac{\iiint \mu H_1 H_2 dv}{\sqrt{\iiint \mu |H_1|^2 dv \times \iiint |H_2|^2 dv}} \tag{3}$$

where $H_1$ and $H_2$ denote the magnetic field vectors of the two coupled lines, respectively. For the microstrip lines, the dominant mode is quasi-TEM mode. The magnetic field can be replaced by corresponding current to estimate the coupling coefficients.

$$k_m = p \times \frac{\int_0^L I_1(x) I_2(x) dx}{\sqrt{\int_0^L |I_1(x)|^2 dx} \sqrt{\int_0^L |I_2(x)|^2 dx}} \tag{4}$$

where $I_1$ and $I_2$ are the current distribution on the two coupled lines, $p$ represents a constant. The coupling region can be separated into two parts, one is from $0$ to $L/3$, and the other is from $L/3$ to $L$. With the coupling region from $L/3$ to $L$, it can be observed that the current distribution of the resonator is odd function, while the current distribution of the feed line is even function. Therefore, according to (4), the magnetic coupling coefficient is zero. The characteristic of electric coupling is similar with the magnetic coupling. So the coupling coefficient of third harmonic is mainly determined by the coupling region from $0$ to $L/3$. To demonstrate this, Figure 4(b) shows the current distribution at the third harmonic. Within the coupling region from BB$'$ to DD$'$, the current on the resonator is odd symmetric with regarding to CC$'$, while the current on the input feed line is even symmetric. According



(a)                                        (b)
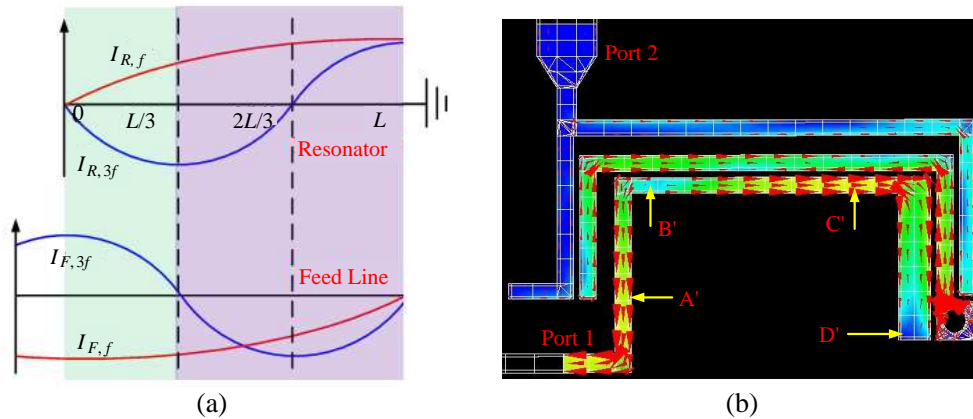
**Figure 4.** (a) Normalized current distribution of the fundamental and the third harmonic at the two coupled lines in theory. (b) Current distribution at the third harmonic.
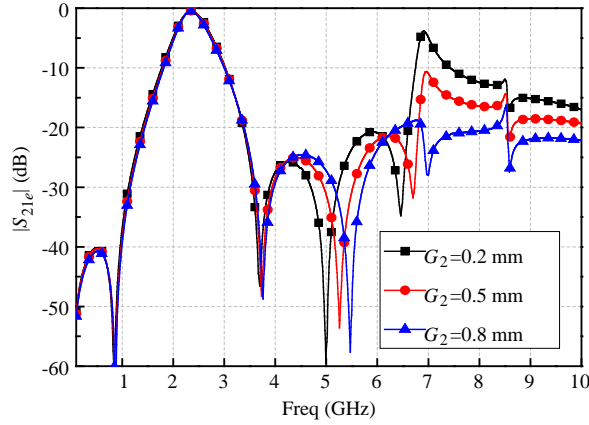
**Figure 5.** Simulated $|S_{21e}|$ against $G_2$.
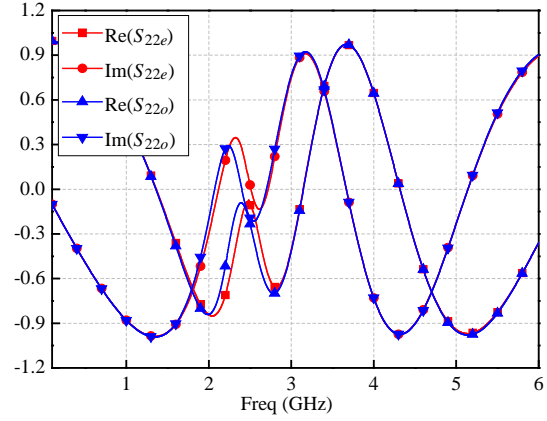


**Figure 6.** Simulated $S_{22e}$ and $S_{22o}$.

to the above analysis, the coupling strength approaches zero. Therefore, the total coupling strength between the feed line and resonator at the third harmonic depends mainly on the region from $AA'$ to $BB'$ and it is controlled by $G_2$. Figure 5 shows the simulated $|S_{21e}|$ of sub-circuit with various $G_2$. It can be observed that when $G_2$ increases, the harmonic can be suppressed because of the insufficient coupling strength at the harmonic frequency. Meanwhile, the coupling strength within passband is nearly unchanged, as the coupling from $AA'$ to $BB'$ accounts a little part to the total coupling from $AA'$ to $CC'$ at the frequency. Compared with the works reported in [12, 13] which use cross-coupling to generate a transmission zero for the second-harmonic suppression enhancement and SIRs to move the harmonic, this work proposed a new mechanism without any extra circuit to obtain a wide stopband. By tuning the above parameters, good filtering performance as well as $S_{11e} = 0$, $S_{22e} = 0$ and wide stopband can be obtained.

In the odd-mode circuit, the gaps, resonator and the feed lines act as an inverter to transform the impedance of $R/2$ to $Z_0$. Since the gaps $G_1$, $G_2$, $G_3$ and $G_4$ are determined by the required bandwidth, $S_{22o}$ can be controlled by $R$ to approximately equal to $S_{22e}$. The simulated $S_{22e}$ and $S_{22e}$ are shown in Figure 6. It can be observed that $S_{22e}$ and $S_{22o}$ are nearly overlapped. By analyzing the real and imaginary parts of $S_{22e}$ and $S_{22o}$, it is found that the difference between $S_{22e}$ and $S_{22o}$ is very slight. According to the equation $S_{23} = (S_{22e} - S_{22o})/2$, good isolation can be obtained.

## 3. FILTER IMPLEMENT

The design procedures of this filtering power divider can be summarized as follows:

1) Determine the length $L_4$ according to the desired centre frequency $f_0$.
2) Fold the resonator at the one third point, adjust the characteristic impedance and coupling gaps to obtain the desired bandwidth.
3) Once the passband performance is determined, $G_2$ is tuned to suppress the harmonic.
4) Choose suitable $R_1$ to maximize the isolation between output ports.
5) Fine tune the dimensional parameters to compensate the discontinuity in the structure and achieve optimum performance.

Based on the previous analysis, a filtering power divider with wide stopband is implemented for demonstration. The substrate has a relative dielectric constant of 3.38 and a thickness of 0.81 mm. The dimensions are obtained as follows (all in mm): $W_1 = 1.86$, $W_2 = 0.5$, $W_3 = 0.5$, $W_4 = 0.5$, $L_1 = 5.1$, $L_2 = 1.5$, $L_3 = 12.4$, $L_4 = 19.7$, $L_5 = 8.3$, $L_6 = 4.6$, $L_7 = 5.5$, $G_1 = 0.2$, $G_2 = 0.6$, $G_3 = 0.2$, $G_4 = 0.6$, $G_5 = 0.2$, $G_1 = 0.2$, $D = 1$, $R_1 = 150\,\Omega$. The overall size of the fabricated filter is $14.5\,\text{mm} \times 16.2\,\text{mm}$ or $0.19\lambda_g \times 0.21\lambda_g$ as shown in Figure 7, where $\lambda_g$ is the guide wavelength at 2.4 GHz. The size is comparable with a classic Wilkinson power divider without filtering responses.
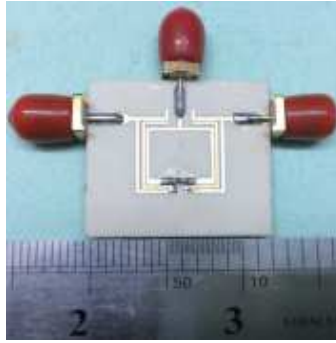
**Figure 7.** Photograph of the fabricated circuit.
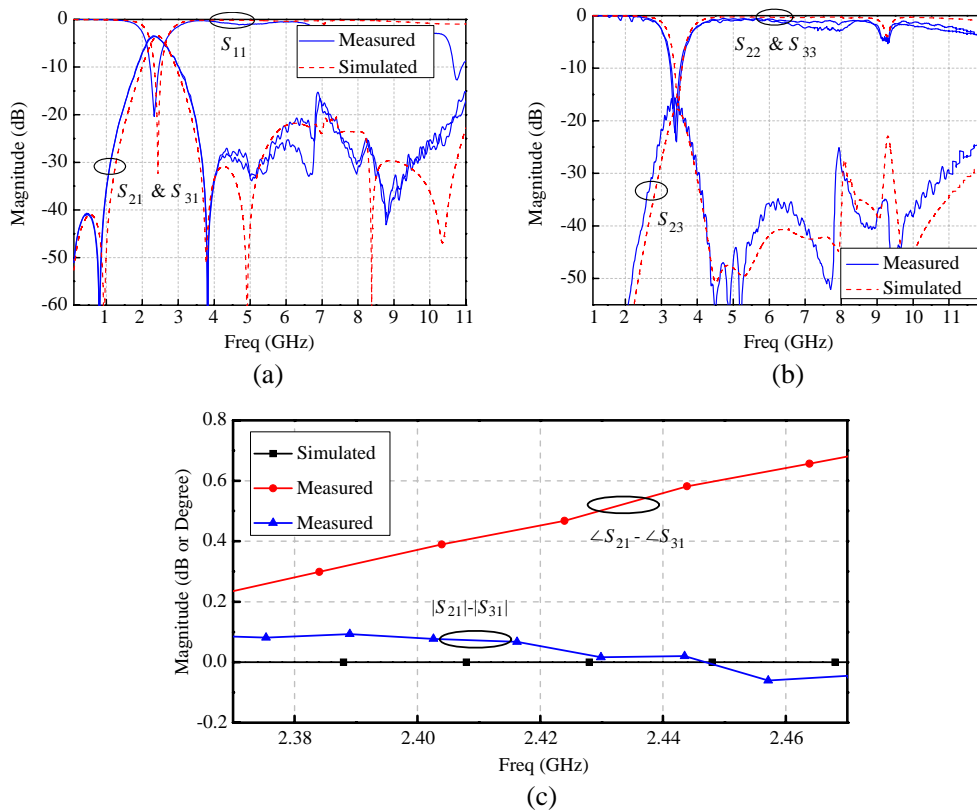


**Figure 8.** Simulated and measured results. (a) $S_{11}$, $S_{21}$ & $S_{31}$. (b) $S_{22}$, $S_{23}$ & $S_{33}$. (c) Amplitude and phase imbalance.

The simulation and measurement are accomplished by using IE3D, ADS and HP N5230 network analyzer, respectively. Figure 8 shows the simulated and measured results. There are some ripples in the measured results, and they are generated since the connector used in the calibration is not very accurate. The measured passband frequency is 2.4 GHz, with the bandwidth of 12.3%. $S_{21}$ and $S_{31}$ including the loss caused by SMA connector are both measured to be $3+0.6$ dB at the center frequency, and the 3 dB is contributed from the power division. The return loss within the passband is 19 dB. Two transmission zeros are generated at both sides of the passband, which improve the roll-off rate. The first one is generated by the weak cross coupling between the input and output lines. The second one is generated since the length of $L_3 + L_7$ is quarter-wavelength near this frequency point; however, it can also be controlled by the weak source-load coupling. Meanwhile, over 15 dB upper stopband suppression is achieved up to 11 GHz ($4.6 f_0$), featuring a wide stopband. Figure 6(b) shows the output

**Table 1.** Comparison with previous work.

| | $f_0$ (GHz) | Filter order | Insertion loss (dB) | Loss tangent of the substrate | In-Band Isolation (dB) | Number of TZs | First Spurious Passband | Size ($\lambda_g \times \lambda_g$) |
|---|---|---|---|---|---|---|---|---|
| [9] | 1.8 | 2 | 3.9 | 0.0019 | > 8 | 2 | $2f_0$ | $0.19 \times 0.29$ |
| [10] | 2 | 4 | 6.4 | 0.0027 | > 15 | 2 | $2f_0$ | $0.49 \times 0.38$ |
| [12] | 0.92 | 3 | 4 | 0.0027 | > 20 | 4 | $3f_0$ | $0.15 \times 0.14$ |
| [13] | 0.9 | 2 | 4.6 | 0.0027 | > 16 | 0 | $5f_0$ | $0.11 \times 0.15$ |
| | | 3 | 5.8 | | > 15 | 0 | $5f_0$ | $0.15 \times 0.17$ |
| | | 4 | 6 | | > 11 | 2 | $5f_0$ | $0.12 \times 0.26$ |
| This work | 2.4 | 1 | 3.6 | 0.0027 | > 16 | 2 | $5f_0$ | $0.19 \times 0.21$ |

TZs denotes number of transmission zeros, $\lambda_g$ is the guide-wavelength of the center frequency.

return loss and isolation. The measured output return losses ($S_{22}$ and $S_{33}$) are better than 20 dB. And the isolation is better than 16 dB within the whole band. The measured amplitude imbalance between two output ports is less than 0.2 dB, and the corresponding phase imbalance is less than 0.8 degree as shown in Figure 6(c), indicating good amplitude and phase balance. Table 1 compares the proposed filtering power divider with previous work. It can be observed that the proposed work realizes a wide stopband and low insertion loss.

## 4. CONCLUSION

A compact power divider with filtering responses has been presented. By controlling the coupling region to realize discriminating coupling, third harmonic has been suppressed, and wide stopband has been obtained. The mechanism has been theoretically analyzed, and both design procedures and experimental results have been provided. Two transmission zeros have been realized near the passband edges, resulting in high selectivity. The compact size, dual functions, simple planar structure as well as high selectivity make it attractive for many applications.

## ACKNOWLEDGMENT

## REFERENCES

1. Li, J. C., Y. L. Wu, Y. A. Liu, J. Y. Shen, S. L. Li, and C. P. Yu, "A generalized coupled-line dual-band Wilkinson power divider with extended ports," *Progress In Electromagnetics Research*, Vol. 129, 197–214, 2012.

2. Liu, W. Q., F. Wei, and X. W. Shi, "A compact tri-band power divider based on triple-mode resonator," *Progress In Electromagnetics Research*, Vol. 138, 283–291, 2013.

3. Chang, L., C. Liao, L.-L. Chen, W. B. Lin, X. Zheng, and Y.-L. Wu, "Design of an ultra-wideband power divider via the coarse-grained parallel micro-genetic algorithm" *Progress In Electromagnetics Research*, Vol. 124, 425–440, 2012.

4. Wu, Y. and Y. Liu, "A unequal coupled-line Wilkinson power divider for arbitrary terminated impedance," *Progress In Electromagnetics Research*, Vol. 117, 181–194, 2011.

5. Gao, L. and X. Y. Zhang, "High selectivity dual-band bandpass filter using a quad-mode resonator with source-load coupling," *IEEE Microw. Wireless Compon. Lett.*, Vol. 23, 474–476, 2013.

6.  Li, J., S. S. Huang, and J. Z. Zhao, "Design of a compact and high selectivity tri-band bandpass filter using asymmetric stepped-impedance resonators (SIRs)," *Progress In Electromagnetics Research Letters*, Vol. 44, 81–86, 2014.

7.  Gao, L., X. Y. Zhang, B.-J. Hu, and Q. Xue, "Novel stub-loaded multi-mode resonators and their applications to various bandpass filters," *IEEE Trans. Microw. Theory Tech.*, Vol. 62, 1162–1172, 2014.

8.  Tang, X. and K. Mouthaan, "Filtering integrated Wilkinson power dividers," *Microw. Opt. Tech. Lett.*, Vol. 52, 2830–2833, 2010.

9.  Li, Y. C., Q. Xue, and X. Y. Zhang, "Single- and dual-band power divider integrated with bandpass filter," *IEEE Trans. Microw. Theory Tech.*, Vol. 61, 69–76, 2013.

10. Shao, J.-Y., S.-C. Huang, and Y.-H. Pang, "Wilkinson power divider incorporating quasi-elliptic filters for improved out-of-band rejection," *Electronics Lett.*, Vol. 47, 1288–1289, 2011.

11. Song, K., S. Hu, Y. Mo, Y. Fan, and C. Zhong, "Novel bandpass-response power divider with high frequency selectivity using centrally stub-loaded resonators," *Microw. Opt. Tech. Lett.*, Vol. 55, 1560–1562, 2013.

12. Zhang, X. Y., K.-X. Wang, and B.-J. Hu, "Compact filtering power divider with enhanced second-harmonic suppression," *IEEE Microw. Wireless Compon. Lett.*, Vol. 23, 483–485, 2013.

13. Chen, C.-F., T.-Y. Huang, T.-M. Shen, and R.-B. Wu, "Design of miniaturized filtering power dividers for system-in-a-package," *IEEE Trans. Compon. Packag. Manufact. Tech.*, Vol. 3, 1663–1672, 2013.

14. Song, K., X. Ren, F. Chen, and Y. Fan, "Ultrawideband notch-band power divider with bandpass response using defect microstrip structure," *Microw. Opt. Tech. Lett.*, Vol. 56, 711–715, 2014.

15. Gao, L. and X. Y. Zhang, "Novel 2 : 1 Wilkinson power divider integrated with bandpass filter," *Microw. Opt. Tech. Lett.*, Vol. 55, 646–648, 2013.

16. Deng, P.-H. and L.-C. Dai, "Unequal Wilkinson power dividers with favorable selectivity and high-isolation using coupled-line filter transformers," *IEEE Trans. Microw. Theory Tech.*, Vol. 60, 1520–1529, 2012.

17. Pozar, D. M., *Microwave Engineering,* 3rd Edition, John Wiley & Sons, 2005.

18. Li, L. and Z. F. Li, "Side-coupled shorted microstrip line for compact quasi-elliptic wideband bandpass filter design," *IEEE Microw. Wireless Compon. Lett.*, Vol. 20, 518–520, 2010.

19. Zhang, X. Y. and Q. Xue, "Harmonic-suppressed bandpass filter based on discriminating coupling," *IEEE Microw. Wireless Compon. Lett.*, Vol. 19, 695–697, 2009.